View metadata, citation and similar papers at core.ac.uk

brought to you by CORE

provided by HKU Scholars Hub

Title	An effective formulation of coupled electromagnetic-TCAD simulation for extremely high frequency onward
Author(s)	Chen, Q; Schoenmaker, W; Meuris, P; Wong, N
Citation	Ieee Transactions On Computer-Aided Design Of Integrated Circuits And Systems, 2011, v. 30 n. 6, p. 866-876
Issued Date	2011
URL	http://hdl.handle.net/10722/155614
Rights	©2011 IEEE. Personal use of this material is permitted. However, permission to reprint/republish this material for advertising or promotional purposes or for creating new collective works for resale or redistribution to servers or lists, or to reuse any copyrighted component of this work in other works must be obtained from the IEEE.

An Effective Formulation of Coupled Electromagnetic-TCAD Simulation for Extremely High Frequency Onward

Quan Chen, *Student Member, IEEE,* Wim Schoenmaker, *Member, IEEE,* Peter Meuris, and Ngai Wong, *Member, IEEE*

***Abstract*—This paper presents an effective formulation tailored for electromagnetic-technology computer-aided design coupled simulations for extremely-high-frequency ranges and beyond (>50 GHz). A transformation of variables is exploited from the starting A-V formulation to the E-V formulation, combined with adopting the gauge condition as the equation for scalar potential. The transformation significantly reduces the cross-coupling between electric and magnetic systems at high frequencies, providing therefore much better convergence for iterative solution. The validation of such transformations is ensured through a careful analysis of redundancy in the coupled system and material properties. Employment of the advanced matrix permutation technique further alleviates the extra computational cost introduced by the variable transformation. Numerical experiments confirm the accuracy and efficiency of the proposed E-V formulation.**

***Index Terms*—A-V solver, coupled simulation, E-V solver, electromagnetic, high frequency, semiconductor.**

I. Introduction

ADVANCED high-speed integrated circuits (ICs), such as radio frequency (RF)/photonic ICs, represent a complicated electromagnetic (EM) system generally consisting of metal or polysilicon interconnects, various semiconductor material systems, and surrounding media, as shown in Fig. 1. Conventional approaches for simulating such complex systems rely on conducting separate characterizations of active devices by technology computer-aided design (TCAD) device models without consideration of electrodynamic effects and finite conductivity of metals, and the passive interconnects by pure EM models simplifying semiconductors to equivalent conducting or dielectric materials. Whereas this "decoupled" characterization suffices at low to medium frequencies, it becomes increasingly questionable beyond extremely high frequency (EHF), e.g., >50 GHz, where the interplay between semiconductor carrier dynamics and EM wave dynamics [1] is prominent. Examples with such strong interplay include metal-insulator-semiconductor interconnects [2], substrate noise isolation structures [3], and through-silicon-via in 3-D integrations [4]. It is therefore suggested that the on-chip actives and passives should no longer be analyzed separately; instead, the critical mixed-signal/RF block must be treated as an entity, and simulated with the full-wave EM physics coupled with the semiconductor carrier dynamics in the design phase to avoid costly mismatch leading to simulation failures or silicon re-spins. This motivates the development of EM-TCAD coupled simulation approach. It should be noted that a coupled full-wave EM-TCAD approach is not demanded in all circumstances. The necessity for the inclusion of the magnetic effects depends on the scale of the structure under consideration. For nano-scale device designs the self-induced magnetic fields may be safely ignored. However, while designing larger parts of the IC, the induced magnetic fields can have a noticeable effect. The eddy current effects in substrates, which take place at still larger scales, are essentially a magnetic field phenomenon. More extensive discussions can be found in [5] and [6].

The objective of coupled simulation is to model and emulate various components (devices, interconnects, substrates, and dielectrics) of on-chip structures within a uniform framework without differentiation in the level of abstraction and/or modeling methodology. Some works have been done on the combination of time-domain full-wave EM analysis and different semiconductor models, mostly via the finite-difference time-domain method (FDTD) [1], [8]. Yet the choice of basic variables in FDTD ($\bar{E}$, $\bar{H}$) is NOT fully compatible with that in TCAD modeling (potentials V) forcing different solution strategies being adopted in different models, which corresponds to a "loosely coupled" scheme. In the frequency domain, the finite-element method (FEM) has been applied to couple the full-wave Maxwell equations with the semiconductor transport equations [2], [9]. Nevertheless, standard FEM aiming at building solution with minimal Galerkin residue may not be able to guarantee exact charge conservation

Manuscript received May 20, 2010; revised August 31, 2010 and October 30, 2010; accepted December 8, 2010. Date of current version May 18, 2011. This work was supported in part by the Hong Kong Research Grants Council under Projects HKU 717407E and 718509E, the University Research Committee of the University of Hong Kong, and in part by the EU Projects CHAMELEON-RF (IST-2004-027378), ICESTARS (IST-FP7/2008/ICT/214911), and the IWT-Medea+Project COSIP-Vlaanderen (IWT-080478). This paper was recommended by Associate Editor R. Suaya.

Q. Chen is with the Department of Computer Science and Engineering, University of California, San Diego, CA 92093 USA (e-mail: quanchen@eee.hku.hk).

W. Schoenmaker and P. Meuris are with MAGWEL NV, Leuven 3000, Belgium (e-mail: wim.schoenmaker@magwel.com; peter.meuris@magwel.com).

N. Wong is with the Department of Electrical and Electronic Engineering, University of Hong Kong, Pokfulam, Hong Kong (e-mail: nwong@eee.hku.hk).

Color versions of one or more of the figures in this paper are available online at http://ieeexplore.ieee.org.

Digital Object Identifier 10.1109/TCAD.2010.2103270

0278-0070/$26.00 © 2011 IEEE

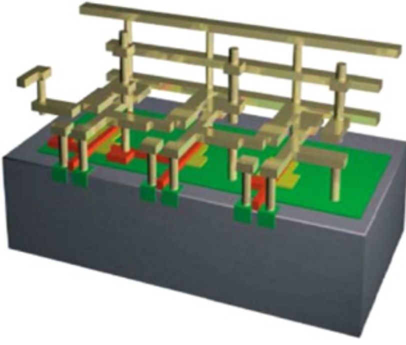

Fig. 1. Typical on-chip structure consisting of metallic interconnects, semiconductor devices, and substrate [7].

and thus may cause spurious oscillations in the numerical solution [10].

A more sophisticated frequency-domain technique for multi-domain (metal, semiconductor and insulator) coupled simulation was proposed in [11] and [12], based on the finite-volume method (FVM) that has built-in guarantee of charge conservation. Instead of the conventional use of electric and magnetic fields ($\bar{E}$ and $\bar{H}$), the technique uses the scalar potential V and vector potential $\bar{A}$ (with $\bar{B} = \nabla \times \bar{A}$) as fundamental variables (denoted as A-V formulation or A-V solver hereafter), and as a consequence provides a convenient, physically consistent and "tightly coupled" interfacing between the full-wave EM model and the TCAD device model. The A-V formulation has been validated for a number of cases in which the simulator results were compared with measured data on test structures developed in industry [13], [14]. The solver has been transferred into a series of commercial tools of MAGWEL, Leuven, Belgium [15].

Despite the attractive performance from DC to tens of GHz, the A-V solver suffers from a slow iterative solution in the high microwave and even terahertz (THz) regimes wherein EM-TCAD coupled simulation capacity is pressingly demanded. The high-frequency difficulty of A-V solver is attributed to the strong cross-couplings between electric and magnetic systems at high frequencies and when metallic materials are involved, which together lead to linear systems with significant off-diagonal dominance that largely affects the convergence of iterative solvers.

In this paper, we propose a new framework of coupled simulation characterized by using V and $\bar{E}$ as basic variables, called the E-V formulation or solver henceforth, in the problem formulation, and by using a modified gauge condition as the equation of V in metals and insulators. The transformation removes much of the undesirable dependency of the cross-couplings on frequency and metal conductivity which is in general a large variable. In this way, the diagonal dominance of resultant Jacobian matrices is improved and the performance of iterative solution is greatly enhanced for EHF problems. Validity of the proposed E-V formulation is proved though examining the redundancy problem specific to coupled simulation and the influence of material properties. Additional cost in computations introduced by the reformulation is well alleviated by the column approximate minimum degree (COLAMD) permutation, rendering the E-V solver an effective tool for generic integrated simulation tasks at sub-THz and THz frequency ranges.

It should be emphasized that the E-V formulation obtained by performing a variable transformation has interesting consequences for microelectronic applications. First, the minimal procedure to identify voltages and currents at contacts and ports is preserved. In other words, the connection to the Kirchhoff variables is straightforward, as was discussed in [12]. Furthermore, the planar technology implies that current elements in the vertical direction are usually over the lengths of the via heights. Consequently, it is a valuable assumption that the vertical component of the vector potential is negligible. This approximation leads to a much smaller size of the set of degrees of freedom and this property is also preserved after the transformation. We also note that the resulting system is not identical to the E-formulation that is often exploited in finite element solvers. The latter often works in the temporal gauge for which $V = 0$ everywhere.

The remaining parts of this paper are organized as follows. Section II briefly reviews the A-V formulation and verifies its feasibility with measurement data. Section III discusses the origin of the difficulty that the A-V solver faces in iterative solution at high frequencies. Formulation and implementation of the proposed E-V solver are detailed in Section IV. An in-depth numerical study of the E-V solver including spectral analyses is provided in Section V to demonstrate the merits of the E-V solver. A conclusion is drawn in Section VI.

II. Review of A-V Formulation

A. A-V Formulation of the Coupled System

In the A-V framework for coupled simulation, the Gauss law is used to solve for the scalar potential V in insulating and semiconducting regions, and the current-continuity equation $\nabla \cdot J + j\omega\rho = 0$ is to be employed to find the V in metals

$$\begin{cases} \nabla \cdot \left[\varepsilon_r \left(\nabla V + j\omega \bar{A}\right)\right] + \rho = 0 & \text{insul. and semi.} \\ \nabla \cdot \left[(\sigma + j\omega\varepsilon_r)\left(\nabla V + j\omega \bar{A}\right)\right] = 0 & \text{metal} \end{cases} \quad (1)$$

where σ, ε_r, and ω denote, respectively, the conductivity, relative permittivity, and frequency. The free charge density is denoted by ρ and in semiconductors $\rho = n + p + N_d$ where N_d is the net doping concentration. This set of equations is often regarded as the electric system.

The current-continuity equation is exploited to solve the electron and hole charge carrier densities, n and p, in the semiconductor region

$$\nabla \cdot \bar{J}_\chi - j\omega q\chi \mp R(n, p) = 0 \quad \chi \in \{n, p\} \quad (2)$$

in which $R(n, p)$ refers to the generation/recombination of carriers and q the elementary charge. The sign $\mp$ is for electrons and holes, respectively. Provided the drift-diffusion model is employed, the semiconductor current is determined by $\bar{J}_\chi = q\mu_\chi\chi\left(-\nabla V - j\omega\bar{A}\right) \pm kT\mu_\chi\nabla\chi$, $\chi \in \{n, p\}$, where μ, k, and T denote the carrier mobility, Boltzmann constant, and temperature, respectively. The Scharfetter-Gummel scheme is applied to discretize (2) [16].

To solve the magnetic vector potential $\bar{A}$, we consider the Maxwell-Ampére equation, which is regarded as the magnetic system

$$\nabla \times \left(\frac{1}{\mu_r} \nabla \times \bar{A} \right) + K(\sigma + j\omega\varepsilon_r)(\nabla V + j\omega\bar{A}) - K\ J_{semi} = 0 \tag{3}$$

where $J_{semi} = J_n + J_p$ denotes the semiconductor current, and K is the dimensionless constant in the scaling scheme [12]. For generic materials of on-chip structures it is safe to set $\mu_r = 1$. Equation (3) itself is not well-defined since the operator $\nabla \times (\nabla \times)$ is intrinsically singular when discretized by FVM. A special treatment in the A-V solver is to subtract (3) by the divergence of the gauge condition

$$\nabla \cdot \bar{A} + \xi K j\omega\varepsilon_r V = 0 \tag{4}$$

which yields

$$\begin{aligned} &\nabla \times \left(\nabla \times \bar{A}\right) - \nabla \left(\nabla \cdot \bar{A}\right) + K(\sigma + j\omega\varepsilon_r) j\omega\bar{A} \\ &+ K(\sigma + j\omega\varepsilon_r)\nabla V - \xi K j\omega\varepsilon_r \nabla V - K J_{semi} = 0 \end{aligned} \tag{5}$$

where ξ is the gauge slider ranging from 0 (Coulomb gauge) to 1 (Lorenz gauge). This regularization procedure recovers a Laplacian-like operator and thus eliminates the singularity.

The task of coupled simulation is to find the simultaneous solution of (1), (2), and (5), which are represented in a condensed notation as

$$\begin{cases} \mathbf{F}\left(V, \{n, p\}, \bar{A}\right) = 0 \\ \mathbf{H}\left(V, \{n, p\}, \bar{A}\right) = 0 \\ \mathbf{G}\left(V, \{n, p\}, \bar{A}\right) = 0. \end{cases} \tag{6}$$

B. Feasibility of the A-V Solver

Using the solver based on computational electrodynamics, we are able to compute the s-parameters by setting up a field simulation of the full structure. This allows us to study in detail the physical coupling mechanisms. As an illustration, we consider two inductors which are positioned on a substrate layer separated by a distance of 14 μm. This structure was processed and characterized and the s-parameters were obtained. It is quite convenient when studying a compact model parameters to obtain a quick picture of the behavior of the structure. For this device a convenient variable is the "gain," which corresponds to the ratio of the injected power and the delivered power over an output impedance [17]

$$G = \frac{P_{in}}{P_{out}}. \tag{7}$$

The structure is shown in Fig. 2.

When computing the s-parameters, we put the signal source on one spiral (port 1) and place 50 Ω impedance over the contacts of the second spiral (port 2). The s_{11}-parameter is shown in Fig. 3 and the s_{12}-parameter is shown in Fig. 4. Finally, the gain plot is shown in Fig. 5. This results shown here have been obtained without any calibration of the material parameters. The silicon is treated "as-is." This means that the substrate and the eddy current suppressing n-wells are dealt with as doped silicon.

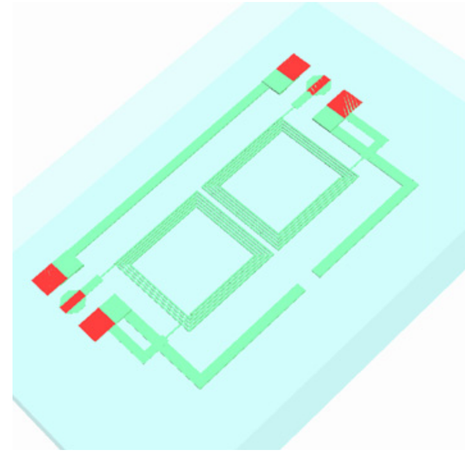

Fig. 2. View on the coupled spiral inductor using the MAGWEL editor.

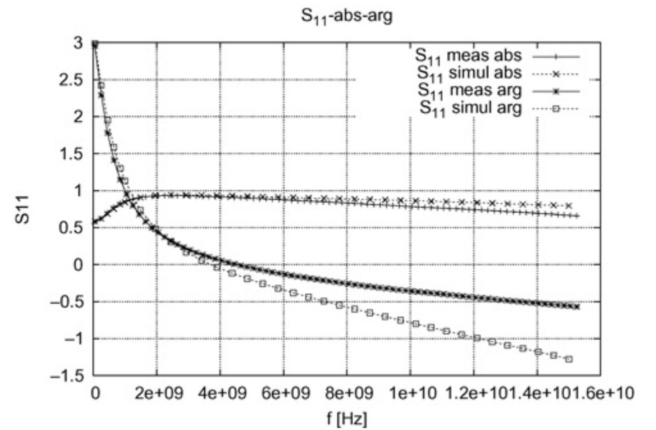

Fig. 3. Comparison of the experiment and simulation results for s_{11}.

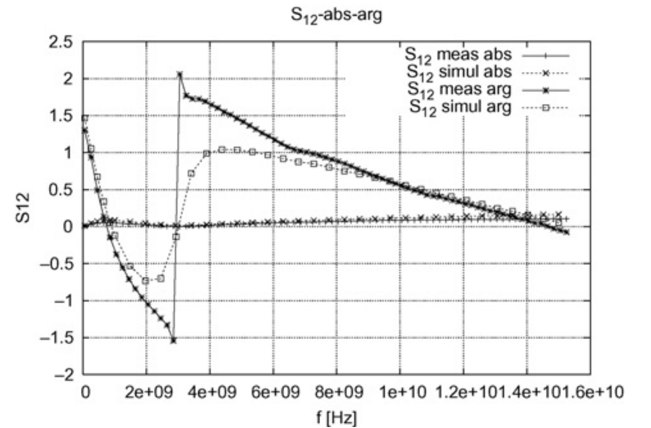

Fig. 4. Comparison of the experiment and simulation results for s_{12}.

III. Origin of the High-Frequency Breakdown of the A-V Solver

The coupled system of equations (6) is intrinsically non-linear when semiconducting regions are present and preferably solved by the Newton's method. The non-linearity arises from the discretization of the current flux along the links of the computational grid. As has been shown in [11], the discretized

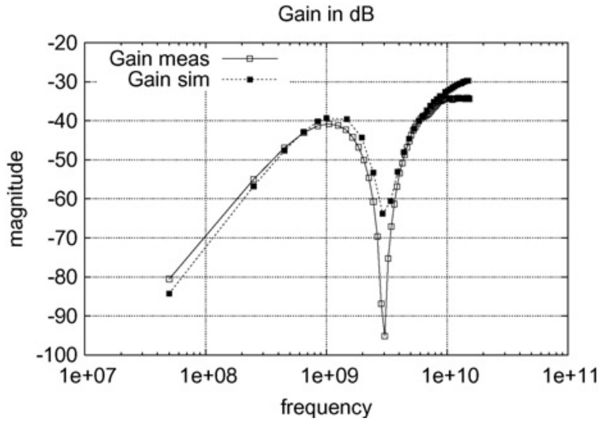

Fig. 5. Comparison of the experimental and simulation results for the gain.

carrier current associated with a link of the grid is

$$J_{\chi ij} = \chi_i B(\mp X_{ij}) - \chi_j B(\pm X_{ij}) \qquad \chi \in \{n, p\} \tag{8}$$

where χ_i and χ_j are the carrier concentrations of the begin and end nodes of the link, and

$$B(z) = \frac{z}{\exp(z) - 1} \tag{9}$$

is the Bernoulli function. The argument $X_{ij} = V_i - V_j + \mathrm{sgn}(ij)\ j\omega h_{ij} A_{ij}$ and V_i, V_j are the nodal voltages and A_{ij} is the projection of the vector potential **A** on the link $<$ ij $>$. Finally, sgn(ij) is $\pm$ depending on the orientation of the link with respect to its begin and end nodes. Evidently, the presence of the Bernoulli function turns the problem into a highly nonlinear one.

Starting from some initial guess, for example the DC solution, the update vector in each Newton's iteration is obtained by solving the sparse linear system

$$MX = b \tag{10}$$

which in detail reads

$$\begin{bmatrix} \frac{\partial \mathbf{F}}{\partial V} & \frac{\partial \mathbf{F}}{\partial \{n,p\}} & \frac{\partial \mathbf{F}}{\partial \bar{A}} \\ \frac{\partial \mathbf{H}}{\partial V} & \frac{\partial \mathbf{H}}{\partial \{n,p\}} & \frac{\partial \mathbf{H}}{\partial \bar{A}} \\ \frac{\partial \mathbf{G}}{\partial V} & \frac{\partial \mathbf{G}}{\partial \{n,p\}} & \frac{\partial \mathbf{G}}{\partial \bar{A}} \end{bmatrix} \begin{bmatrix} \Delta V \\ \Delta \{n, p\} \\ \Delta \bar{A} \end{bmatrix} = - \begin{bmatrix} \mathbf{F}(V, \{n, p\}, \bar{A}) \\ \mathbf{H}(V, \{n, p\}, \bar{A}) \\ \mathbf{G}(V, \{n, p\}, \bar{A}) \end{bmatrix}. \tag{11}$$

The numerical difficulty of the A-V solver can be revealed by analyzing the magnitudes of the matrix entries in (11), which are mainly dependent on the electric properties of materials and the frequency under consideration. The differential operators (∇, $\nabla\cdot$, $\nabla\times$) are usually of order one with spatial scaling. In the electric sector (1) the magnitude of the cross-coupling of $\bar{A}$ to V is

$$\frac{\partial \mathbf{F}}{\partial \bar{A}} = \nabla \cdot \left[j\omega\left(\sigma + j\omega\varepsilon_r\right)\right] \sim O\left(j\omega\left(\sigma + j\omega\varepsilon_r\right)\right) \tag{12}$$

where $O(\cdot)$ denotes the order of the magnitude, and in the magnetic sector (5) the magnitude of the cross-coupling of V to $\bar{A}$ is

$$\frac{\partial \mathbf{G}}{\partial V} = \left[K(\sigma + j\omega\varepsilon_r)\nabla - \xi K j\omega\varepsilon_r \nabla\right] \sim O\left(K(\sigma + j\omega\varepsilon_r)\right). \tag{13}$$

Although the cross-couplings between $\bar{A}$ and V tend to vanish at zero frequency, they become dominant for frequencies in the higher GHz range, especially when the structure includes metallic conductors that have large conductivity σ and skin effects are desired to be computed such that surface-impedance models can be obtained. When solved by the widely-used Krylov subspace methods such as GMRES, these significant off-diagonal blocks will impose negative effects to the convergence rate through inducing undesirable spectral distribution in the preconditioned system matrix. For instance, the popular ILU preconditioner and its variants compute the incomplete L and U factors of M such that

$$M = LU + E \tag{14}$$

where E is the error matrix. Then an iterative solver effectively deals with the preconditioned matrix

$$(LU)^{-1} M = I + U^{-1} L^{-1} E. \tag{15}$$

For diagonally dominant matrices, L and U are well conditioned and the size (2-norm) of $U^{-1}L^{-1}E$ remains reasonably bounded, which confines the eigenvalues of the preconditioned matrix within a small neighborhood of 1 and allows a fast convergence of Krylov subspace methods. When the matrix M lacks diagonal dominance, L^{-1} or U^{-1} may have large norms, rendering the "preconditioned" error matrix $U^{-1}L^{-1}E$ of large size and thus adding large perturbations to the identity matrix [18]. This large perturbation causes the eigenvalues dispersed and spread far away from each other, resulting in slow down or even failure of the convergence of iterative solution. As a consequence, the A-V solver becomes increasingly inefficient, if not impossible, in EHF scenarios wherein coupled simulation is demanded to capture the complicated interplay between EM wave and semiconductor carrier transport.

IV. E-V Formulation

From a modeling perspective, the above intensive cross-coupling arises from explicitly separating the electric field (more precisely the electric field in the metals) into its static component from V and dynamic component from $\bar{A}$, and associating them with equal weightings that have magnitudes depending on the frequency and metal conductivity. To reduce the weight of cross-coupling terms, we reformulate the coupled system using the scalar potential V and the electric field $\bar{E}$ via the variable transformation

$$\bar{E} = -\nabla V - j\omega\bar{A}. \tag{16}$$

The coupled system of (1), (2), and (5) under this transformation changes into

$$\mathbf{F}' : \begin{cases} \nabla \cdot \left(\varepsilon_r \bar{E}\right) + \rho = 0 & \text{semi. and insul.} \\ \nabla \cdot \left[\left(\sigma + j\omega\varepsilon_r\right)\bar{E}\right] = 0 & \text{metal} \end{cases} \tag{17a}$$

$$\mathbf{H}' : \nabla \cdot \bar{J}_\chi - j\omega q\chi \mp R(n, p) = 0 \quad \chi \in \{n, p\} \tag{17b}$$

$$\mathbf{G}' : \nabla \times \left(\nabla \times \bar{E}\right) - \nabla\left(\nabla \cdot \bar{E}\right) + Kj\omega(\sigma + j\omega\varepsilon_r)\bar{E} \\ -\nabla\left(\nabla^2 V\right) - \xi K\omega^2 \nabla\left(\varepsilon_r V\right) + Kj\omega\bar{J}_{semi} = 0 \tag{17c}$$

where $\bar{J}_\chi = q\mu_\chi \chi \bar{E} \pm kT\mu_\chi \nabla\chi,\ \chi \in \{n, p\}$ accordingly. Note that here we only consider $\bar{E}$ as a variable transformation of $\bar{A}$ instead of an independent physical quantity.

The transformation from A-V to E-V immediately removes the conductance-dependent cross-coupling of V from (17c). Yet little improvement has been made to (17a) wherein the cross-coupling coefficients of $\bar{E}$ still have undesirable dependence on σ and ω. A detailed analysis of the coupled system in the next subsection however indicates that we are allowed to exploit, instead of the Gauss law (17a) (as well as the current-continuity), the transformed gauge condition to determine the scalar potential in the metal and insulator regions (but not in the semiconductor regions), which reads

$$\nabla^2 V + \xi K \omega^2 \varepsilon_r V + \nabla \cdot \bar{E} = 0. \tag{18}$$

This way, the cross-couplings of $\bar{E}$ have magnitudes of order one, and are not growing any more with the large value of σ and frequency in the bulk of metallic materials. Whereas the conversion from A-V solver to E-V solver looks promising, there are certain subtleties that require special attention to guarantee a correct implementation of the E-V solver.

A. *Redundancy in Coupled System*

It is a unique feature for coupled EM-TCAD simulation to look for a simultaneous solution of the following system, which consists of the Gauss law, the current-continuity law, and the Maxwell-Ampére law

$$\nabla \cdot \bar{D} - \rho = 0 \tag{19a}$$

$$\nabla \cdot \bar{J} = 0 \tag{19b}$$

$$\nabla \times \bar{H} - \bar{J} = 0 \tag{19c}$$

where $\bar{J}$ represents the total current including the conduction and the displacement parts. In the A-V formulation all unknowns are expressed in terms of potentials V and $\bar{A}$, and a gauge condition is required to eliminate the well-known gauge freedom to ensure a unique solution

$$\nabla \cdot \bar{A} + f = 0 \tag{20}$$

where f can be an arbitrary function of V and $\bar{A}$.

It is straightforward to see (19), more exactly (19b) and (19c) is redundant by taking the divergence on both sides of (19c) [19]. Conventional TCAD device simulation or full-wave EM simulation alone is free of this redundancy, in that the former uses only (19a) and (19b) to solve for V and ρ (n and p) without $\bar{A}$, while the latter uses only (19c) and (20) to look for V and $\bar{A}$ in the absence of ρ [which is recovered later via (19a)]. When the A-V solver has to deal with the combined system of (19b) and (19c) that is fundamental to describe the field-carrier interaction, it employs a specific technique to address the redundancy problem, which, as mentioned above, is to subtract (19c) by the divergence of the gauge condition, yielding

$$\nabla \times \bar{H} - \bar{J} - \nabla \cdot \left(\nabla \cdot \bar{A} + f\right) = 0. \tag{21}$$

There are several points in (21) that deserve attention.

1) The system of (19b) and (21) is not redundant as long as the gauge condition is not explicitly involved in the system of equations.
2) Though the gauge condition does not participate in the solution procedure, it should serve as an implicit constraint and be recovered from the solution thereby obtained.

Taking divergence on (21) and together with (19b), we have

$$\nabla^2 \left(\nabla \cdot \bar{A} + f\right) = 0 \tag{22}$$

which is essentially a Laplace's equation. In numerical theory, it is known that for a Laplace's equation $\nabla^2\phi = 0$ in some domain Ω, the solution will be zero everywhere in Ω provided the boundary condition $\phi|_{\partial\Omega} = 0$ is applied. Hence, the requirement of the second point is that the gauge condition must be set equal to zero at the boundary of the simulation domain. This is done in the discretization of (21), wherein the evaluations of $\nabla \cdot \bar{A} + f$ are forced to be equal to zero by the discretization scheme for the nodes bouncing on the boundary of the simulation domain. In other words, the gauge condition will be automatically recovered over the usual Maxwell-Ampére equation for the whole domain provided that the current-continuity equation is solved.

The above discussion shows the way how the A-V solver deals with the redundancy arising when different systems of equations are coupled together, wherein the current-continuity equation is solved explicitly for V with the gauge condition being an implicit constraint. Alternatively, one could choose the gauge condition as the equation of V constrained by the current conservation. This change requires the current-continuity equation being removed from the system of equations, otherwise the system will become redundant again since the gauge condition is enforced explicitly and implicitly at the same time. The removal of current-continuity equation as a consequence requires the removal of charge density ρ from the unknown list for an equal counting of equations and unknowns. Such removal is applicable in the metallic and insulating regions in which ρ is able to be recovered by the Gauss law, while not in the semiconductors in which the carrier concentrations n and p are of fundamental interest and cannot be recovered from merely the field variables.

As a result, in the E-V solver (18) can be exploited to solve for V in the metals and insulators (though not entirely, see the next section), while (17a) remains the one we should use in the semiconducting regions. Note that the gauge condition will still be recovered in the semiconductors given the fact that the gauge condition is set zero at all nodes surrounding the semiconductors. In addition, using (17) in the semiconductors will not introduce large cross-coupling terms as the relative permittivities of semiconducting materials are generally of order one.

B. *Issues of Material Properties*

Depending on the electric properties of the materials under investigation (metal or insulator or material interfaces), there are still subtle distinctions in the appropriate formulation of

gauge condition that should be employed as the equation of V, i.e., (18) in the E-V solver. For nodes in the bulk of metals as well as material interfaces except semiconductor/insulator interfaces, the governing equation is essentially the current-continuity equation; the Gauss equation will come into use only when the (surface) charge density is demanded in post-process steps. Therefore, the equation in the E-V solver for these nodes is exactly (18), which together with (17c) are equivalent to the current-continuity equation (1) in the A-V solver.

The situation is slightly different for the insulating regions. The current-continuity is now trivial (0 = 0) and the (small-signal) free charge density is zero by definition. Therefore, there is no need to recover the current-continuity equation and only the Gauss's equation must be recovered. Although applying the gauge condition to find out V remains possible, such choice will induce certain numerical difficulty, especially for the insulators with homogeneous dielectric constants. This is because, due to the homogeneity of dielectric constants, solution of (18) in the bulk of insulators has to obey a stronger requirement of demanding $\nabla^2 V + Kj\omega\varepsilon_r V = 0$ and $\nabla \cdot \bar{E} = 0$ simultaneously. Direct application of (18) will cause non-uniqueness in the solution and render the system matrix highly ill-conditioning. As a result, the ordinary Gauss equation remains an appropriate choice to determine the scalar potential in the insulators, no matter homogeneous or inhomogeneous

$$\nabla \cdot \left(\varepsilon_r \bar{E}\right) = 0. \tag{23}$$

The nodes at semiconductor/insulator interfaces are classified as semiconductor nodes for which it is natural to apply the original Gauss equation (17a).

C. Boundary Conditions

Boundary conditions for the E-V solver are derived from its A-V counterpart through the transformation relation (16). The underlying principle is to minimize the coupling between the simulation domain and the rest of the world.

As done in the A-V solver [11], [12], we divide the boundary of the simulation domain into two parts: contact regions and non-contact regions. The contacts allow currents, and thus energy, to enter and leave the simulation domain, wherein the constant voltage condition is applied. The remainder, the non-contact boundary, is characterized by demanding that the outward-pointing normal component of $\bar{E}$ vanishes, i.e., $\bar{E}_n = 0$. This leads to the boundary condition of the electric system for non-contact boundary nodes

$$\nabla \cdot \left[\left(\sigma + j\omega\varepsilon_r\right) \bar{E}\right] = 0. \tag{24}$$

The boundary condition (24) introduces again a σ-dependent coupling in some circumstances, i.e., for boundary nodes attached by metallic cubes. Their contribution to undesirable cross-couplings, however, is much lower than that in the A-V formulation, wherein all nodes attached by metallic cubes have to be taken into account.

For the magnetic sector, the similar requirement of $\bar{B}_n = 0$ is applied to keep all magnetic fields remain inside the simulation domain. This forces a zero tangential component of $\bar{A}$ since $\bar{B} = \nabla \times \bar{A}$, namely, $\bar{A}_t = 0$, which holds for both the contact and non-contact boundaries. In light of (16), the boundary condition of magnetic system should be

$$\bar{E}_t = -\nabla V_t. \tag{25}$$

The above condition implies the unknowns associated with the boundary links, which are part of degrees of freedom in the E-V solver but not in the A-V solver, can be substituted by the corresponding nodal unknowns of V in the solution phase and recovered later by post-processing. This way, the total number of unknowns are identical for both the A-V and E-V solvers.

It should be emphasized that above selection of the boundary conditions represents a particular choice which was motivated by upgrading standard TCAD simulations into the electromagnetic regime. However, there is nothing "fundamental" about this choice. One may equally well choose radiative boundary conditions or Neumann-type boundary conditions for the vector potential. The preferred choice depends on the problem under consideration. Here, it is important to note that when discussing the A-V solver and the E-V solver, the *same* physical boundary conditions are used.

D. Implementation Details

The full system of equations of the E-V solver is laid out in (26)

$$\mathbf{F}' : \begin{cases} \nabla \cdot \left[\left(\sigma + j\omega\varepsilon_r\right) \bar{E}\right] - \rho = 0 & \text{boundary} \\ \nabla \cdot \left(\varepsilon_r \bar{E}\right) - \rho = 0 & \text{semi. and insul} \\ \nabla^2 V + \xi K \omega^2 \varepsilon_r V + \nabla \cdot \bar{E} = 0 & \text{remaining regions} \end{cases} \tag{26a}$$

$$\mathbf{H}' : \nabla \cdot \bar{J}_\chi - j\omega q \chi \mp R(n, p) = 0 \qquad \chi \in \{n, p\} \tag{26b}$$

$$\mathbf{G}' : \nabla \times \left(\nabla \times \bar{E}\right) - \nabla\left(\nabla \cdot \bar{E}\right) + Kj\omega(\sigma + j\omega\varepsilon_r)\bar{E} - \nabla\left(\nabla^2 V\right) - \xi K \omega^2 \nabla\left(\varepsilon_r V\right) + Kj\omega \bar{J}_{semi} = 0. \tag{26c}$$

Similar to (11), a linear system $MX = b$ is solved at each Newton's step, in which M results from the FVM discretization of the Jacobian of (26).

It is convenient to upgrade the A-V solver to include an E-V solver by exploiting the following 4-step solution strategy.

1) Map $\bar{A} - V$ variables onto $\bar{E} - V$ variables via (16).
2) Apply the E-V solver to compute the update vector $\left[\Delta V, \Delta\bar{E}\right]^T$ in the Newton's iteration.
3) Map $\left[\Delta V, \Delta\bar{E}\right]^T$ onto $\left[\Delta V, \Delta\bar{A}\right]^T$.
4) Update the A-V system.

Using this approach, the data structure in the original A-V solver is unaltered and the switching between the A-V and E-V solvers is easy to realize. This is beneficial in that, as shown in Section IV, the A-V and E-V solvers are suitable to work complementarily with the former at low frequencies and the latter at high frequencies, and thus switching between solvers may be needed in a wide-band simulation.

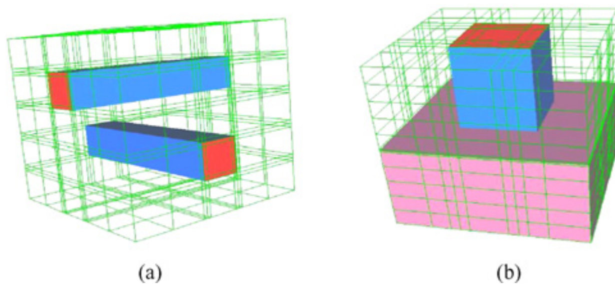

Fig. 6. (a) Cross wire structure. Simulation domain is $10 \times 10 \times 10\,\mu\text{m}^3$ and the cross sections of metal wires are $2 \times 2\,\mu\text{m}^2$. $\sigma = 5.96 \times 10^7$ S/m. FVM discretization generates 1400 nodes and 3820 links. (b) Metal plug structure. Simulation domain is $10 \times 10 \times 10\,\mu\text{m}^3$ the cross section of metal plug is $4 \times 4\,\mu\text{m}^2$. $\sigma = 3.37 \times 10^7$ S/m. A uniform doping of $N_D = 1 \times 10^{24}$ is used. FVM discretization generates 1300 nodes and 3540 links.

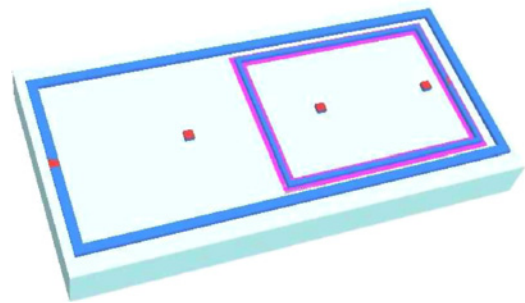

Fig. 7. Substrate noise isolation structure. A deep n-well (DNW) (pink region) is implanted in the p-type substrate to isolate analog circuits from digital noise sources. Simulation domain is $100 \times 50 \times 11\,\mu\text{m}^3$. $\sigma = 3.37 \times 10^7$ S/m. A user-defined doping profile is adopted. FVM discretization generates 6300 nodes and 13 540 links.

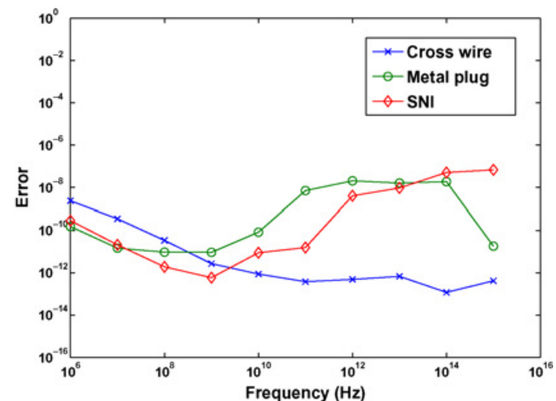

Fig. 8. Differences between the A-V and E-V solvers for the testing structures (with direct solver).

E. Matrix Permutation

Despite the attractive reduction in the magnitudes of cross-couplings, the E-V transformation introduces more non-zero fill-ins into the off-diagonal block of $\frac{\partial \mathbf{G}}{\partial V}$ through the term $\nabla\left(\nabla^2 V\right)$ in (26c). The increased amount of fill-ins from A-V to E-V formulations is approximately $10\times$ the number of boundary links. Inferior sparsity burdens the construction of preconditioner as well as subsequent iterations, limiting the applications of E-V solver to relatively small-sized problems.

To enhance the performance of the E-V solver, the COLAMD permutation [20] is applied to the system matrix M, which computes a permutation vector p such that the (incomplete) LU factorization of $M(:, p)$ tends to be much sparser than that of M. This way, building popular ILUT preconditioners with small threshold becomes possible for M in the order of tens of thousands. The subsequent iteration also speeds up owing to the improved sparsity of the computed LU factors.

V. Numerical Results

The proposed E-V solver as well as its A-V counterpart, on which MAGWEL's softwares are based, are implemented and compared in MATLAB. The "de Mari" scaling scheme [12] is adopted. For simplicity, the Coulomb gauge ($\xi = 0$) is adopted throughout the numerical experiments. Three structures are tested to demonstrate the efficiency of the E-V solver: 1) a cross wire structure consisting only of passives as shown in Fig. 6(a); 2) a metal plug structure consisting of both passives and actives as shown in Fig. 6(b); and 3) a practical substrate noise isolation (SNI) structure as shown in Fig. 7. The iterative solutions are computed by GMRES with ILUT preconditioners. All programming and simulations were done on a 3.2 GHz 16-Gb-RAM Linux-based server.

A. Accuracy of E-V Solver

Fig. 8 verifies the accuracy of E-V solver in comparison with the A-V solver at frequencies ranging from 10^6 Hz to 10^{15} Hz for the three test benches. This frequency range covers a wide spectrum from medium radio frequency to visible light. Direct solver (Gaussian elimination) is used to solve the linear equations at each Newton's iteration. The accuracy is measured by the relative error between the whole internal state space solution of the A-V and E-V solvers $\text{err} = \|X_{EV} - X_{AV}\|_2 / \|X_{AV}\|_2$, $X = \left[V; n; p; \bar{A}\right]$. It is seen that the E-V solver is in an excellent agreement with the A-V solver throughout the testings, which is expected from a mathematical perspective since no approximation is introduced in the variable and equation transformations. The slight fluctuations in the curves are due to the final precisions of Newton's method and vary among solvers even when the same convergence criterion is applied. Fig. 9 visualizes the current density inside the substrate of the SNI structure, demonstrating a clear isolation effect for the part of analog circuits from external digital noises.

B. Spectral Analyses

To investigate the influence of increasing frequency on the A-V and E-V solvers, we plot in Figs. 10 and 11 the eigenvalues of the Jacobian matrices preconditioned by ILUT(10^{-6}) for the metal plug structure at four different frequencies. The norms of L^{-1} and U^{-1} of each solver are also computed in Table I.

At relatively low frequency (10^6 Hz), the off-diagonal blocks in (12) and (13) are of small sizes and so are the norms of the inverses of incomplete factors L and U in (15). The eigenvalues of the preconditioned matrix from the A-V solver

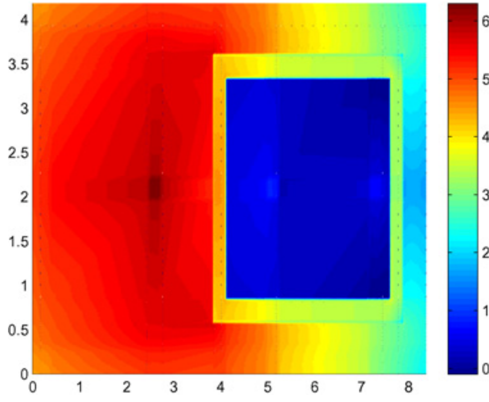

Fig. 9. Current density at the middle layer of the substrate of SNI structure (shown in log10 scale).

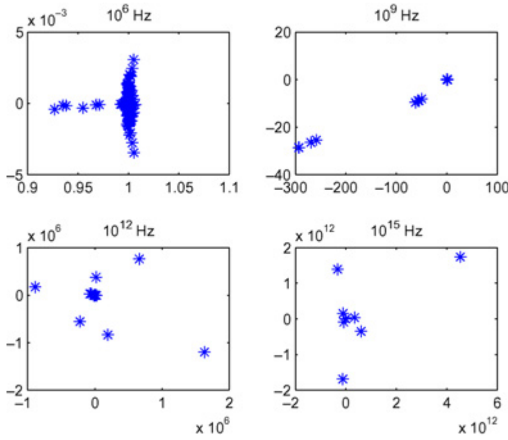

Fig. 10. Eigenvalue distribution of the preconditioned Jacobian matrices of A-V solver at different frequencies.

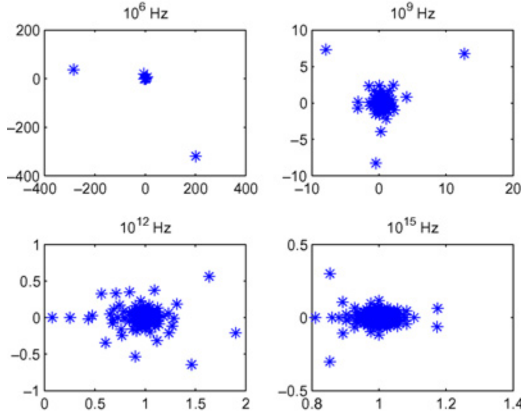

Fig. 11. Eigenvalue distribution of the preconditioned Jacobian matrices of E-V solver at different frequencies.

are then tightly clustered around the point 1 in favor of a fast convergence of iterative solution. As frequency increases, the spectra of the preconditioned matrices have eigenvalue clusters with continuously enlarging radii and separations among each other, reflecting an increasing perturbation to the identity matrix as the result of increasing off-diagonal dominance. This is also confirmed by looking into the growing sizes of U^{-1}

TABLE I
NORMS OF L^{-1} AND U^{-1} COMPUTED FOR THE A-V AND E-V SOLVERS [ILUT(10^{-6})]

Frequency	A-V		E-V	
	$\|L^{-1}\|$	$\|U^{-1}\|$	$\|L^{-1}\|$	$\|U^{-1}\|$
10^6 Hz	1.55×10^1	4.82	9.15×10^1	1.67×10^7
10^9 Hz	1.32×10^1	4.87×10^2	4.37×10^1	3.82×10^4
10^{12} Hz	2.50×10^1	1.75×10^7	2.89×10^1	1.16×10^2
10^{15} Hz	2.42×10^2	1.15×10^{11}	1.52×10^1	5.15

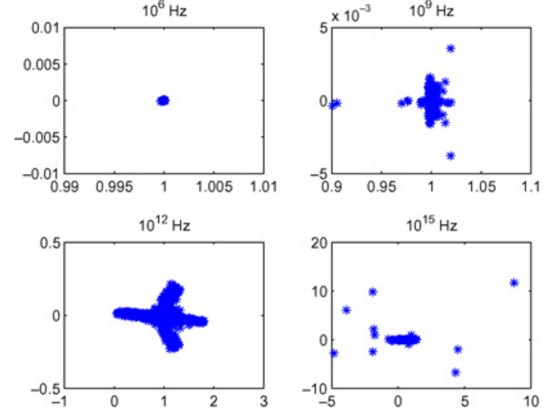

Fig. 12. Eigenvalue distribution of the preconditioned Jacobian matrices of A-V solver at different frequencies (no metal).

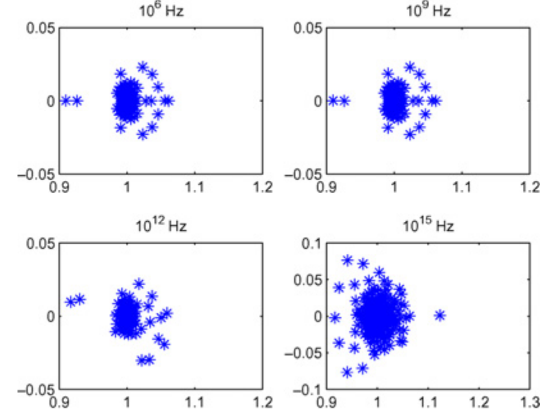

Fig. 13. Eigenvalue distribution of the preconditioned Jacobian matrices of E-V solver at different frequencies (no metal).

in Table I. It therefore suggests a poor iterative performance for the A-V solver at high frequencies when Krylov subspace methods are applied, whose convergence behaviors are closely related to the relative radii of eigenvalue clusters and their separations of the preconditioned matrix [21]. The enlargements of cluster radii and separations are proportional to the increases of frequency.

Compared to that of the A-V solver, the spectral distribution of the preconditioned system of E-V solver has a roughly opposite trend along with the rising frequency. The eigenvalues are clustered more loosely at low frequencies, while becoming increasingly concentrated around 1 at higher frequencies, due to the growing contribution from the term of $Kj\omega(\sigma + j\omega\varepsilon_r)\bar{E}$ in (26c) improving diagonal dominance. Such concentration

TABLE II
ITERATIVE PERFORMANCE OF A-V AND E-V SOLVERS FOR THE CROSS WIRE STRUCTURE [ILUT(10^{-6}), TIME UNIT: S]

Freq.	A-V(ORIG)			A-V(AMD)			A-V(DS)	E-V(ORIG)			E-V(AMD)			E-V(DS)
	t_{pre}	N_{it}	$t_{per\ it}$	t_{pre}	N_{it}	$t_{per\ it}$		t_{pre}	N_{it}	$t_{per\ it}$	t_{pre}	N_{it}	$t_{per\ it}$	
10^6	48.34	5	0.37	11.22	5	0.38			NC			NC		
10^7	62.15	6	0.34	12.68	7	0.37		179.16	546	1.51	49.88	515	1.01	
10^8	62.96	11	0.41	12.91	12	0.39		179.49	130	1.11	45.73	91	0.71	
10^9	77.59	27	0.42	14.80	35	0.41		163.00	17	1.09	43.15	14	0.67	
10^{10}	105.06	43	0.73	20.77	167	0.50		163.73	9	1.09	38.01	8	0.65	
10^{11}		NC			NC		12.76	155.41	8	1.03	38.09	7	0.63	15.08
10^{12}		NC			NC			154.45	7	1.01	38.50	7	0.61	
10^{13}		IP			NC			154.52	7	1.08	38.77	6	0.57	
10^{14}		IP			IP			150.29	6	0.98	34.55	6	0.57	
10^{15}		IP			IP			127.37	5	1.01	28.64	6	0.51	

TABLE III
ITERATIVE PERFORMANCE OF A-V AND E-V SOLVERS FOR THE METAL PLUG STRUCTURE [ILUT(10^{-6}), TIME UNIT: S]

Freq.	A-V(ORIG)			A-V(AMD)			A-V(DS)	E-V(ORIG)			E-V(AMD)			E-V(DS)
	t_{pre}	N_{it}	$t_{per\ it}$	t_{pre}	N_{it}	$t_{per\ it}$		t_{pre}	N_{it}	$t_{per\ it}$	t_{pre}	N_{it}	$t_{per\ it}$	
10^6	100.02	5	0.57	34.83	5	0.62	37.39		NC			NC		50.12
10^7	146.18	6	0.54	53.71	7	0.65			NC			NC		
10^8	156.44	10	0.60	62.01	11	0.68		616.12	187	2.11	136.12	141	1.11	
10^9	200.28	22	0.69	62.50	27	0.66		455.02	81	1.81	129.19	51	0.91	
10^{10}	207.16	102	0.73	69.39	165	0.72		442.65	21	1.73	128.94	18	0.92	
10^{11}		NC			NC			440.56	13	1.72	100.18	12	0.80	
10^{12}		NC			NC			369.19	11	1.39	85.50	11	0.78	
10^{13}		IP			NC			363.20	9	1.32	83.16	10	0.78	
10^{14}		IP			IP			362.21	7	1.23	83.18	7	0.81	
10^{15}		IP			IP			309.64	5	1.10	83.20	6	0.74	

TABLE IV
ITERATIVE PERFORMANCE OF A-V AND E-V SOLVERS FOR THE SNI STRUCTURE [ILUT(10^{-4}), TIME UNIT: S]

Freq.	A-V(ORIG)			A-V(AMD)			A-V(DS)	E-V(ORIG)			E-V(AMD)			E-V(DS)
	t_{pre}	N_{it}	$t_{per\ it}$	t_{pre}	N_{it}	$t_{per\ it}$		t_{pre}	N_{it}	$t_{per\ it}$	t_{pre}	N_{it}	$t_{per\ it}$	
10^6	1298.45	8	2.57	252.83	9	2.12	943.01		NC			NC		1391.67
10^7	1506.15	32	3.54	349.11	41	3.45			NC			NC		
10^8	2112.06	100	4.60	539.78	140	4.08			NC			NC		
10^9		NC			NC			17347.12	141	11.12	770.81	101	3.62	
10^{10}		NC			NC			13556.65	71	9.34	598.76	70	3.49	
10^{11}		NC			NC			9342.33	47	9.02	474.05	44	3.28	
10^{12}		IP			NC			8006.09	40	8.62	427.25	36	3.20	
10^{13}		IP			IP			7681.85	36	8.00	394.00	32	3.01	
10^{14}		IP			IP			7262.10	19	7.68	318.64	18	2.85	
10^{15}		IP			IP			7245.72	16	6.11	301.66	15	2.79	

of eigenvalues greatly facilitates the convergence of iterative methods and thus suggests enhanced performances for the E-V solver at high-frequency scenarios.

Similar experiments are conducted in Figs. 12 and 13 to examine the role of metal conductivity. The metal plug structure is used again, but with the metallic part replaced by insulating materials, rendering the structure consisting of only insulators and semiconductors. Horizontal comparisons for the A-V solver show that, whereas at sufficiently high frequencies the eigenvalues still disperse, the degree of dispersion is reduced by a great extent. This confirms that the presence of metallic conductors with large conductivity is one origin of the numerical difficulty of A-V solver at high frequencies. The eigenvalues of E-V solver are in a similar distribution over the four testing frequencies, suggesting roughly constant performance in iterative solution.

C. Performance Comparisons

Detailed comparisons between the A-V and E-V solvers for their performances in iterative solution are tabulated in Tables II–IV. A relative tolerance of 10^{-10} and a maximum number of iterations of 1000 are used in GMRES. The high accuracy used in iterative solution is intended to minimize the number of necessary Newton iterations to as close as with direct solver, so as not to complicate the analysis by the issues related to the convergence rate of Newton's method. Successful solutions with convergence achieved are shown with the time for building preconditioner, the number of iterations and the time per iteration. Unsuccessful solutions, according to the reasons of failure, are marked as "NC" (no convergence within the maximum number of iterations) or "IP" (ill-conditioned preconditioner). The iterative solvers with and without COLAMD pre-processing are labeled as "AMD"

and "ORIG," respectively. The runtimes of direct solver (at 10 GHz) are also shown with the label of "DS" for reference.

For all the three structures, the A-V solver exhibits deteriorated performances as frequency increases, and tends to break down at frequencies beyond (tens of) GHz for requiring either a large number of iterations or high-quality preconditioners that are costly to generate ("UV catastrophe"). The E-V solver fails to converge for low frequencies ("IR singularity") but in contrast to the A-V solver, performs increasingly well with growing frequency. These results are consistent with the above spectral analysis and confirm the merit of the E-V solver as a capable tool in EHF applications. Meanwhile, it suggests that the A-V and E-V solvers have complementary preferable frequency ranges and thus are suitable to work together to provide a truly wide-band coupled simulation framework.

As frequency increases, calculating ILUT preconditioners are generally more time-consuming for the A-V solver, while less for the E-V solver, which may be attributed to their opposite behaviors in terms of diagonal dominance. Without matrix permutation, the constructions of preconditioners for the E-V solver are several times slower than that of the A-V solver due to a higher number of matrix fill-ins introduced by the $\nabla(\nabla^2 V)$ term. This prevents the E-V solver from being applied to simulate large-scale problems. As a remedy, application of the COLAMD permutation in the E-V solver provides a remarkable reduction ($\sim$20X for the SNI example) in the computational cost of preconditioner and a moderate reduction (>2X for the SNI example) in the cost of following iterations, rendering the overall cost of E-V solver comparable even with that of the COLAMD-permuted A-V solver, for which the improvement is less significant because of its inherently better sparsity. Besides, an increased number of iterations are observed for the COLAMD-permuted A-V solver compared to the original version, offsetting its gain in preconditioner computations. It turns out that the E-V solver combined with COLAMD is the most robust and efficient tool for coupled simulations at EHF and beyond.

VI. Conclusion

An effective E-V formulation was proposed, with dedication to the simultaneous simulation of full-wave EM and semiconductor dynamics for EHF regime onward. The underlying idea was to reformulate the conventional A-V formulation via variable and equation transformations, which removed the undesirable dependences of cross-couplings on frequency and metal conductivity, and as a consequence brings substantial improvement into the efficiency of iterative solution at high frequencies. From a spectral perspective, the improved diagonal dominance ameliorates the concentric appearance of eigenvalues of the preconditioned Jacobian matrix, by which a fast convergence of iterative solution was achieved. The equation transformation from the Gauss equation to the gauge condition was rigorously validated by a careful investigation of the redundancy in coupled system and the influence of material properties. The COLAMD matrix permutation technique was applied to offset the additional cost introduced by the E-V reformulation, rendering the E-V solver comparably efficient with its A-V counterpart. Numerical experiments have confirmed the superior performance of the proposed method with frequency up to optical range.

Acknowledgment

Discussions with N. Banagaaya and W. Schilders are highly appreciated.

References

[1] K. J. Willis, J. S. Ayubi-Moak, S. C. Hagness, and I. Knezevic, "Global modeling of carrier-field dynamics in semiconductors using EMC-FDTD," *J. Comput. Electron.*, vol. 8, no. 2, pp. 153–171, Jun. 2009.

[2] G. F. Wang, R. W. Dutton, and C. S. Rafferty, "Device-level simulation of wave propagation along metal-insulator-semiconductor interconnects," *IEEE Trans. Microw. Theory Tech.*, vol. 50, no. 4, pp. 1127–1136, Apr. 2002.

[3] P. C. Yeh, H. K. Chiou, C. Y. Lee, J. Yeh, D. Tang, and J. Chern, "An experimental study on high-frequency substrate noise isolation in BiCMOS technology," *IEEE Electron Device Lett.*, vol. 29, no. 3, pp. 255–258, Mar. 2008.

[4] C. Xu, H. Li, R. Suaya, and K. Banerjee, "Compact AC modeling and analysis of Cu, W, and CNT based through-silicon vias (TSVs) in 3-D ICs," in *Proc. IEEE IEDM*, Dec. 2009, pp. 521–524.

[5] W. Schoenmaker, P. Meuris, E. Janssens, W. Schilders, and D. Ioan, "Modeling of passive-active device interactions," in *Proc. 37th ESSDERC*, Sep. 2007, pp. 163–166.

[6] N. Nastos and Y. Papananos, "RF optimization of MOSFETs under integrated inductors," *IEEE Trans. Microw. Theory Tech.*, vol. 54, no. 5, pp. 2106–2117, May 2006.

[7] S. Kapora, M. Stuber, W. Schoenmaker, and P. Meuris, "Substrate noise isolation characterization in 90 nm CMOS technology," in *Proc. User Track IEEE DAC*, Jul. 2009.

[8] R. O. Grondin, S. M. El-Ghazaly, and S. Goodnick, "A review of global modeling of charge transport in semiconductors and full-wave electromagnetics," *IEEE Trans. Microw. Theory Tech.*, vol. 47, no. 6, pp. 817–829, Jun. 1999.

[9] F. Bertazzi, F. Cappelluti, S. D. Guerrieri, F. Bonani, and G. Ghione, "Self-consistent coupled carrier transport full-wave EM analysis of semiconductor traveling-wave devices," *IEEE Trans. Microw. Theory Tech.*, vol. 54, no. 4, pp. 1611–1617, Apr. 2006.

[10] W. Schoenmaker, W. Magnus, P. Meuris, and B. Maleszka, "Renormalization group meshes and the discretization of TCAD equations," *IEEE Trans. Comput.-Aided Design*, vol. 21, no. 12, pp. 1425–1433, Dec. 2002.

[11] P. Meuris, W. Schoenmaker, and W. Magnus, "Strategy for electromagnetic interconnect modeling," *IEEE Trans. Comput.-Aided Design*, vol. 20, no. 6, pp. 753–762, Jun. 2001.

[12] W. Schoenmaker and P. Meuris, "Electromagnetic interconnects and passives modeling: Software implementation issues," *IEEE Trans. Comput.-Aided Design*, vol. 21, no. 5, pp. 534–543, May 2002.

[13] *CODESTAR: Compact Modeling of On-Chip Passive Structures at High Frequencies* [Online]. Available: http://www.magwel.com/codestar

[14] *Chameleon-RF: Comprehensive High-Accuracy Modeling of Electromagnetic Effects in Complete Nanoscale RF Blocks* [Online]. Available: http://www.chameleon-rf.org

[15] MAGWEL [Online]. Available: http://www.magwel.com

[16] D. L. Scharfetter and H. K. Gummel, "Large scale analysis of a silicon read diode oscillator," *IEEE Trans. Electron Devices*, vol. 16, no. 1, pp. 64–77, Jan. 1969.

[17] A. M. Niknejad and R. G. Meyer, "Analysis, design and optimization of spiral inductors and transformers for Si RF ICs," *IEEE J. Solid-State Circuits*, vol. 33, no. 10, pp. 1470–1481, Oct. 1998.

[18] Y. Saad, *Iterative Methods for Sparse Linear Systems*. Boston, MA: PWS, 1996.

[19] P. Enders, "Underdeterminacy and redundance in Maxwell's equations equations: Origin of gauge freedom—transversality of free electromagnetic waves—Gaugefree canonical treatment without constraints," *Electron. J. Theor. Phys.*, vol. 6, no. 22, pp. 135–166, Oct. 2009.

[20] T. A. Davis, J. R. Gilbert, S. I. Larimore, and E. G. Ng, "A column approximate minimum degree ordering algorithm," *ACM Trans. Math. Softw.*, vol. 30, no. 3, pp. 353–376, 2004.

[21] S. L. Campbell, I. C. F. Ipsen, C. T. Kelley, and C. D. Meyer, "GMRES and the minimal polynomial," *BIT*, vol. 36, pp. 32–43, 1996.

Quan Chen (S'09) received the B.S. degree in electrical engineering from Sun Yat-Sen University, Guangzhou, China, in 2005, and the M.Phil. and Ph.D. degrees in electronic engineering from the University of Hong Kong, Pokfulam, Hong Kong, in 2007 and 2010, respectively.

Currently, he is a Post-Doctoral Fellow with the Department of Computer Science and Engineering, University of California, San Diego. His research interests include high-frequency electromagnetic analysis of very large scale integration and electromagnetic transactions on computer-aided design coupled simulation. His current research interest includes parallel SPICE simulation.

Wim Schoenmaker (M'01) received the B.S. degree in physics and the M.S. degree in theoretical physics, both from the Free University of Amsterdam, Amsterdam, The Netherlands, in 1975 and 1979, respectively, and the Ph.D. degree in theoretical high-energy physics from the University of Groningen, Groningen, The Netherlands, in 1983.

From 1983 to 1987, he held post-doctoral positions in particle physics with the University of Kaiserslautern, Kaiserslautern, Germany, and the University of Leuven, Leuven, Belgium, where his research interests concerned lattice gauge theories and statistical physics and computing. In this research, the exploration and exploitation of large-scale computer resources has been a major theme. From 1987 to 2003, he was with the Interuniversity Microelectronic Center (IMEC), Leuven, where he has been working on the development of numerical simulation tools and computer-aided design (CAD) tools for the study and design of electronic devices at the sub-micrometer level. From 1993 to 2003, he was heading the Technology CAD Group, IMEC, which is in charge of the software for process and device simulation as well as the integration of these tools into advanced technology CAD systems for microelectronic engineering. Besides the work dealing with the development of CAD tools for the microelectronic industry, there is also original research performed in the field of quantum transport in ultrasmall devices, as well as the development of a microscopic theory for electromigration phenomena. In 2003, he co-founded MAGWEL NV, Leuven, that provides software solutions for the simulation of interconnects and integrated passives on the medium and high-frequency range. Since 2003, he has been the CTO with MAGWEL NV. He is the (co-)author of 140 peer-reviewed journal papers and conference contributions, three patents, and one book and two book chapters.

Dr. Schoenmaker was an Associate Editor of the IEEE TRANSACTIONS ON COMPUTER-AIDED DESIGN from 1998 to 2005.

Peter Meuris received the M.E. degree in electrical engineering and the Ph.D. degree in plasma physics, both from the University of Ghent, Ghent, Belgium, in 1993 and 1997, respectively.

He joined the Interuniversity Microelectronic Center (IMEC), Leuven, Belgium, in 1999, performing research on electromagnetic modeling of on-chip interconnects using a computer-aided design approach. In April 2003, he founded MAGWEL NV, Leuven, as an IMEC spinoff. He has authored or co-authored 40 papers on electromagnetism, and deliverables in research projects and has been a reviewer for several international journals. His main topic of interest includes electromagnetic technology computer-aided design.

Ngai Wong (S'98–M'02) received the B.Eng. degree with first class honors and the Ph.D. degree, both in electrical and electronic engineering, from the University of Hong Kong, Pokfulam, Hong Kong, in 1999 and 2003, respectively.

He was an Intern with Motorola, Inc., Hong Kong, from 1997 to 1998, specializing in product testing. He was a Visiting Scholar with Purdue University, West Lafayette, IN, in 2003. Currently, he is an Associate Professor with the Department of Electrical and Electronic Engineering, University of Hong Kong. His current research interests include very large scale integration (VLSI) model order reduction and simulation, digital filter design, sigma-delta modulators, and optimization problems in communication and VLSI applications.